



From neural stem cells to glioblastoma: A natural history of GBM recapitulated in vitro

Cristina Almengló¹ | Pilar Caamaño² | Máximo Fraga³ | Jesús Devesa⁴ |
José A. Costoya¹  | Víctor M. Arce¹ 

¹Molecular Oncology Laboratory MOL, Departamento de Fisiología, Centro Singular de Investigación en Medicina Molecular e Enfermedades Crónicas CiMUS, Facultade de Medicina, Universidade de Santiago de Compostela, Instituto de Investigación Sanitaria de Santiago de Compostela IDIS, Santiago de Compostela, Spain

²Fundación Publica Galega de Medicina Xenómica, Santiago de Compostela, Spain

³Departamento de Anatomía Patolóxica e Ciencias Forenses, Universidade de Santiago de Compostela, Santiago de Compostela, Spain

⁴Research and Development, Medical Center Foltra, Teo, Spain

Correspondence

José A. Costoya and Víctor M. Arce, Molecular Oncology Laboratory MOL, Departamento de Fisiología, Centro Singular de Investigación en Medicina Molecular e Enfermedades Crónicas CiMUS, Facultade de Medicina, Universidade de Santiago de Compostela, Instituto de Investigación Sanitaria de Santiago de Compostela IDIS, Santiago de Compostela, Spain.

Email: josea.costoya@usc.es and victor.arce@usc.es

Víctor M. Arce, Molecular Oncology Laboratory MOL, Departamento de Fisiología, Centro Singular de Investigación en Medicina Molecular e Enfermedades Crónicas CiMUS, Facultade de Medicina, Universidade de Santiago de Compostela, Instituto de Investigación Sanitaria de Santiago de Compostela IDIS, Santiago de Compostela, Spain.

Email: victor.arce@usc.es

Funding information

European Regional Development Fund, Grant/Award Number: ED431G/05; Xunta de Galicia, Grant/Award Number: 2014-PG029; University of Santiago de Compostela, Grant/Award Number: 2018-PU001; Secretaría de Estado de Investigación, Desarrollo e Innovación, Grant/Award Number: PI15/01129

Abstract

Due to its aggressive and invasive nature glioblastoma (GBM), the most common and aggressive primary brain tumour in adults, remains almost invariably lethal. Significant advances in the last several years have elucidated much of the molecular and genetic complexities of GBM. However, GBM exhibits a vast genetic variation and a wide diversity of phenotypes that have complicated the development of effective therapeutic strategies. This complex pathogenesis makes necessary the development of experimental models that could be used to further understand the disease, and also to provide a more realistic testing ground for potential therapies. In this report, we describe the process of transformation of primary mouse embryo astrocytes into immortalized cultures with neural stem cell characteristics, that are able to generate GBM when injected into the brain of C57BL/6 mice, or heterotopic tumours when injected IV. Overall, our results show that oncogenic transformation is the fate of NSC if cultured for long periods in vitro. In addition, as no additional hit is necessary to induce the oncogenic transformation, our model may be used to investigate the pathogenesis of gliomagenesis and to test the effectiveness of different drugs throughout the natural history of GBM.

KEYWORDS

glioblastoma, metastasis, neural stem cells, replicative senescence

1 | INTRODUCTION

Glioblastoma (GBM) is the most malignant and highly aggressive type of gliomas, which accounts for almost 50% of primary malignant brain tumours in adults. However, it still carries a poor prognosis, with a 5-year survival of 4.7%, due to its aggressive and invasive nature, and its remarkable heterogeneity (Jacob et al., 2020; Joshi et al., 2015; Louis et al., 2016; Ostrom et al., 2018; Patel et al., 2014). These characteristics complicate the development of effective therapeutic strategies and compel the need for more trustworthy models to study the disease and test new drugs and therapies.

In vitro cultures are widely employed as suitable models to investigate both the pathogenesis and the therapeutics of GBM, although these models are imperfect for several reasons. Different lines of immortalized glioma cells, such as U87, U251, T98G, or CT-2A have been widely used for more than 30 years (Caragher et al., 2019; Xie et al., 2015). However, although the use of cell lines has provided valuable knowledge about GBM, they undergo profound phenotypical changes when grown as monolayers, and fail to develop the defining morphological features of GBM tumours when injected in vivo. These cells also exhibit markedly different responses to cytotoxic treatments than those observed in patients, and controversy regarding their origins has recently appeared (Allen et al., 2016).

On the other hand, the use of patient-derived cells has become the gold standard of GBM preclinical studies, mainly to test personalized therapies, and a library of annotated and validated cell lines derived from surgical samples of GBM patients has been recently created (Jacob et al., 2020; Xie et al., 2015). It is expected that the use of validated cells, together with novel culture systems that better recapitulate the complex reality of brain tumours growing in situ (Caragher et al., 2019) may provide a more suitable model for preclinical GBM research in the next future. However, despite their clear benefits over some current models, these models still have important limitations when investigating the pathogenesis of GBM, as they are established from already developed tumours, either spontaneously generated in a patient or experimentally induced in a cell line or laboratory animal. Therefore, it is very difficult to recapitulate the natural history of the oncogenic process and identify molecular targets involved in the early development of the disease.

In this study, we describe a novel cellular model that allows investigating the transformation of mouse neural stem cells (NSC) into aggressive GBM with metastatic capacity. Our results show that oncogenic transformation occurs in immortalized NSC because of long-term passaging in vitro, and without the need of any external hit other than the factors presented in a standard culture media. Furthermore, this transformation occurred with a 100% frequency, indicating that it is the fate of immortalized NSC in vitro, at least under our experimental conditions. Whether a similar process may occur in vivo, as a consequence of the dysregulation of the neurogenic niche, remains to be elucidated.

2 | MATERIALS AND METHODS

2.1 | Cell cultures

Immortalized NSC were generated from 13.5 dpc (day post coitum) C57BL/6 mice embryos, as previously described (Almengló et al., 2020; Seoane et al., 2017). Briefly, pregnant C57BL/6 mice were sacrificed at 13.5 dpc and uterine horns were then dissected. Each embryo was separated from its placenta and embryonic sac and transferred to an individual petri dish with Dulbecco's modified Eagle's medium (DMEM; Sigma-Aldrich). The head of each embryo was individually transferred to fresh Petri dishes, and brains were then isolated, finely minced, and dissociated by mechanical shearing, followed by filtration through a 40-micron mesh. Cells were plated in Falcon polystyrene culture dishes (BD Biosciences) and grown in DMEM supplemented with 10% foetal bovine serum (Thermo Fisher Scientific), 2 mM glutamine, 2.5 U/ml penicillin, and 2.5 mg/ml streptomycin (all from Thermo Fisher Scientific). Cultures were maintained at 37°C in a humidified atmosphere of 5% CO₂. This method has been proved to consistently yield more than 95% of glial fibrillary acidic protein (GFAP) + primary mouse embryo astrocytes (MEA) (Almengló et al., 2017, 2020; Seoane et al., 2017). Immortalization of primary MEA was achieved by using the 3T3 protocol (Todaro & Green, 1963) with appropriate modifications (Almengló et al., 2020). Cells were transferred to new dishes with fresh medium every 3 days, with the same cell density ($3 \times 10^3/\text{cm}^2$) seeded in every transfer. Continual cell passaging was used to generate long-term cultures of low passage (LP)-immortalized cells (below 20 passages) or high passage (HP)-immortalized cells (40–100 passages) (see Figure 1 for further details). Both the immortalization protocol and the long-term maintenance of immortalized cells were carried out in DMEM. Formation of neurospheres was induced by using a modification of the neurosphere assay (Almengló et al., 2017; Azari et al., 2011). In this case, cells growing in DMEM were trypsinized and transferred to fresh polystyrene culture dishes (approximately $3 \times 10^5/\text{dish}$) with semisynthetic (neurobasal) medium supplemented with 100 U/ml penicillin, 100 µg/ml streptomycin, 1% Gibco B27 supplement, 10 ng/ml bFGF, and 10 ng/ml EGF (NBE conditions) (Lee et al., 2006). As immortalization occurred with a 100% frequency, and no differences were observed in the outcome of the cells, results obtained with different batches of immortalized NSC are presented throughout this study.

To ensure the detection of the immortalized cells after injection in mice, and to rule out a spontaneous origin of the generated tumours, luminescence and fluorescence reporter systems were developed. To create the luminescence reporter, the pBABE-puro-Luc vector was transfected into Phoenix ecotropic retroviral packaging cells (a gift from C. Watzl) (Swift et al., 2001) by using the JetPEI polyplus transfection system (Illkirch, France). Retrovirus-containing supernatant was collected 48 h after transfection and used to infect immortalized cell cultures, using polybrene (5 µg/ml) as transduction enhancer. Cells were then selected for 48 h with 2.5 µg/ml puromycin, and infection efficiency was measured by

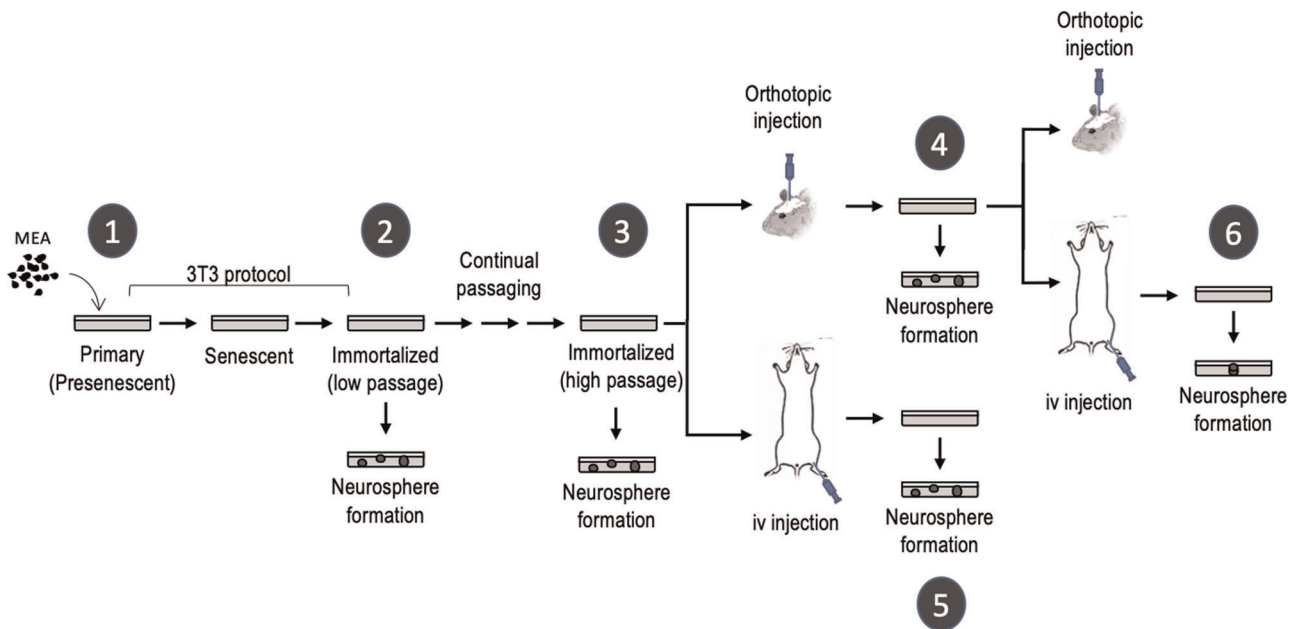


FIGURE 1 Experimental design used for the generation of the different cell types investigated. Primary cultures of MEA obtained from 13.5 dpc mouse embryos (1) were submitted to a 3T3 protocol, resulting in the generation of immortalized NSC (low passage) (2). Immortalized NSC can proliferate indefinitely, leading to high-passage-immortalized NSC (3). Orthotopic injection of high-passage-immortalized NSC in mice resulted in the generation of GBM (4); while IV injection of high-passage-immortalized NSC in the tail vein resulted in the formation of heterotopic (metastatic) tumours (5). Finally, formation of heterotopic (metastatic) tumours was also observed after IV injection of GBM-derived cells (6). As indicated in the figure, the capacity to form neurospheres was assessed in every cell type. GBM,; MEA, mouse embryo astrocyte; NSC,;

quantifying the luciferase activity using an optical in vivo imaging system (IVIS Spectrum, Perkin-Elmer). A red fluorescence reporter gene was created by replacing the sequence coding for GFP in a pMSCV PIG vector (Puro IRES GFP empty vector) with the sequence encoding the monomeric far-red fluorescent protein TagFP635 from a pTagFP635-C vector. The new vector was transfected into Phoenix ecotropic retroviral packaging cells and the supernatant was used to infect immortalized cells, as indicated before.

2.2 | Generation of orthotopic tumours

Orthotopic tumours were generated by stereotaxic injection of immortalized NSC. Six-week-old C57BL/6 male mice were anesthetized by intraperitoneal injection of a ketamine (80–100 mg/kg) and xylazine (16–20 mg/kg) mixture and returned to a holding cage briefly before being placed on a stereotaxic frame (David Kopf Instruments). The surgical area was carefully scrubbed, and a sagittal incision was made through the scalp. The periosteum was then retracted by gently rubbing and microinjections were made in the brain parenchyma according to a topographical map (Paxinos & Franklin, 2019) (coordinates: anterior -0.2 mm, lateral 1 mm from bregma and depth 2.2 mm from the skull surface) by using a 25-gauge needle (Hamilton 7001 syringe, Hamilton Company). The needle was gently inserted into the skull opening, retracted to accommodate the injection volume ($5 \mu\text{l}$), and the cell suspension (1×10^5 cells) was

slowly injected. Once the microsyringe was removed, the head skin was sutured with surgical silk. Mice were monitored for anaesthetic recovery and postsurgical pain. To obtain GBM-derived cell cultures, tumours were finely minced and dissociated by mechanical shearing as indicated above. Cell cultures were grown in DMEM as described and neurosphere generation was induced by placing the cells in NBE conditions.

2.3 | Generation of heterotopic (metastatic) tumours

To investigate the hematogenous dissemination of either HP-immortalized cells or GBM-derived cells, 3-week-old male mice were anesthetized with isoflurane (3% v/v), placed in a restrainer, and injected with the corresponding cell suspension (3×10^5 cells diluted in $500 \mu\text{l}$ of saline solution). Cells were injected in the caudal vein with a 25-gauge needle, and animals were monitored for 5–10 min to ensure haemostasis. Cell cultures from macroscopic metastatic lung tumours were performed as described. After carefully dissecting the tumours from the surrounding tissue, they were finely minced and dissociated by mechanical shearing. Cell cultures were grown in DMEM and neurosphere generation was induced by placing the cells in NBE conditions.

To test the presence of micrometastasis in several organs, cell cultures from lung, kidney, spleen, brain, bone marrow, testicles, and

liver were performed. Except for bone marrow, tissues were finely minced and dissociated as described. From bone marrow cultures, femora and tibiae of the mice were harvested and flushed using phosphate-buffered saline (PBS) in a 1-ml syringe with a 25-gauge needle. Cells were collected by centrifugation and seeded. In all cases, cultures were grown in DMEM, and neurosphere generation was induced by placing the cells in NBE conditions.

2.4 | In vivo imaging

For in vivo monitoring of tumoral growth, luciferin was injected intraperitoneally at a dose of 10 μ l/g body weight. Mice were then anesthetized with isoflurane (3% v/v) and placed on the imaging stage of an optical imaging system (IVIS Spectrum). Images were collected every minute from 15 to 30 min after luciferin injection, and photon emission was quantified using Living Image Software (Living Image 3.1; PerkinElmer).

2.5 | Immunocytochemistry

For immunocytochemical analysis, approximately 5×10^3 cells were seeded in glass coverslips, placed in 24-multiwell plates, and incubated for 24 h, as described above. Cells were then fixed in 96% ethanol for 1 h, rinsed in PBS, and permeabilized by adding 250 μ l of 0.1% TritonX-100, 0.3% bovine serum albumin for 1 h. After rinsing the cells three times in PBS, an overnight incubation at 4°C was performed with the following primary antibodies: anti-glial fibrillary acidic protein (Dako, Agilent Technologies; ready to use), anti-myelin basic protein (MBP; dilution 1:2000; Dako, Agilent Technologies), anti-nestin (dilution 1:200; Merck Millipore), anti-RFP (β IIIIT; dilution 1:2000; Dako, Agilent Technologies), and anti-Ki67 (dilution 1:1000; Seven Hills Bioreagents). Positive cells were detected with a universal second antibody kit that uses a peroxidase-conjugated labelled dextran polymer (EnvisionPlus, Dako, Agilent Technologies) and photographed with an Olympus BX43 camera (Olympus Optical Co.).

2.6 | Immunohistochemistry

For histological evaluation, tissues were fixed by immersion in 10% buffered formalin for 24 h, then dehydrated in ethanol (70%) for 24 h, and embedded in paraffin using a standard procedure. Serial 4- μ m sections were consecutively cut with a microtome (Leica Microsystems GmbH) and transferred to adhesive-coated slides. Immunohistochemistry was performed with a universal second antibody kit that uses a peroxidase-conjugated labelled-dextran polymer (Envision Plus, Dako). The following primary antibodies were used: anti-glial fibrillary acidic protein (Dako, Agilent Technologies; ready to use), anti-myelin basic protein (Dako, Agilent Technologies; dilution 1:2000), anti-nestin (Merck Millipore; dilution 1:200), anti-

RFP (Dako, Agilent Technologies; dilution 1:2000), and anti-Ki67 (dilution 1:1000; Seven Hills Bioreagents). Overnight incubation at 4°C was performed with every antibody. For negative controls, each staining run was incubated with normal rabbit serum instead of the primary antibody. Counterstaining was performed with hematoxylin-eosin staining.

2.7 | Real-time polymerase chain reaction (PCR)

Total RNA was isolated from the different cell cultures by using TRIzol (Invitrogen). cDNA was synthesized with the Transcriptor first-strand cDNA synthesis kit (Roche Diagnostics), and real-time PCR was performed using SYBR Green Master Mix (Applied Biosystems) with an iCycler equipment (7500 PCR Systems, Applied Biosystems). Samples were denatured at 95°C for 15 s, annealed at 55 s, for 15 s, and extended at 72°C for 40 s, for a total of 40 cycles. The Sequence detection software 1.4 (Applied Biosystems) was used for quantification, using GAPDH as control. The oligonucleotide sequences used are: GAPDH forward: AGGTCGGTGAACGGATTG; GAPDH reverse: GGGGTCGTTGATGGCAACA; GFAP forward: TCGCTTCTCTGAACGCTTCTCG; GFAP reverse: TCTGAACGC TGTGACTTGGAGTTCC; MBP forward: CCAAGTTCACCCCTACT CCA; MBP reverse: AGGGGAAGAAAACAAAGGA; nestin forward: CCCTGAAGTCGAGGAGCTG; nestin reverse: CTGCTGCACCT CTAAGCGA. Statistical analysis was performed with the nonparametric test of Kolmogorov-Smirnov. Statistical significance was established at $p < .05$.

2.8 | Metaphase chromosome preparation

Metaphase spreads were prepared after treating the cells with colcemid (0.1 μ g/ml; Sigma-Aldrich) for 7 h. Cells were then incubated in hypotonic buffer (0.05 M KCl, 0.0034 M trisodium citrate) for 20 min at 37°C and fixed in 75% methanol, 25% acetic acid. Cells were then spotted onto microscope slides and stained with 2% Wright stain (0.1 μ g/ml; Sigma-Aldrich) in Gurr buffer, pH 7.0 (Invitrogen). Metaphase chromosomes were scored using a Leica 2005 microscope under a 100X oil objective lens. At least 50 metaphases were analysed from three independent experiments.

2.9 | Cell proliferation assay

Cells were seeded at 10×10^3 (primary), 5×10^3 (immortalized low passage) or 2.5×10^3 (immortalized HP, GBM-derived and metastasis-derived) and grown in DMEM for 1, 3, 5 or 7 days. At these times, cells were fixed and stained with 0.1% violet crystal (Sigma-Aldrich) for 30 min and then washed with PBS to remove the dye excess. Dye content was quantified in a spectrophotometer. To determine the rate of BrdU incorporation, 10^6 cells were seeded in poly-L-lysine-coated slides (1 ml/slide) and

TABLE 1 Generation of GBM in mice after orthotopic injection of primary (1), low passage-immortalized NSC (2) or high-passage-immortalized NSC (3) (see Section 2 for further details)

Mice No.	Cell type (passages)	Time to tumour
1	1 (-)	No tumour
2	1 (-)	No tumour
3	2 (15)	No tumour
4	2 (15)	No tumour
5	3 (40)	3.5 months
6	3 (40)	3.5 months
7	3 (40)	3.5 months
8	3 (60)	3.5 months
9	3 (60)	3.5 months
10	3 (60)	3.5 months
11	3 (90)	3.5 months
12	3 (90)	3.5 months
13	3 (90)	3.5 months

maintained for 24 h. Cells were grown in the presence of BrdU (10 mM; Sigma-Aldrich) for 2.5 h, and BrdU+ cells were detected by immunocytochemistry using a monoclonal antibody (dilution 1:2000; BD Biosciences). Representative images were captured with an Olympus DP72 camera (Olympus Optical Co.), and the number of BrdU+ cells was quantified in 10 random fields per slide.

2.10 | Dot blot assay

A multiplexed protein detection kit (C-Series Human/Mouse AKT Pathway Phosphorylation Array C1, RayBiotech) was used to investigate the existence of changes in the signalling machinery among the different cell types generated. All procedures were performed according to the manufacturer's instructions. Briefly, cells were washed with ice-cold PBS and solubilized in lysis buffer. Cell lysates were then centrifuged (14,000 rpm, 5 min, 4°C) and protein concentration was determined using the Bradford assay (Bio-Rad Laboratories). Membranes were blocked for 30 min at room temperature and incubated overnight at 4°C with 200 µg of each sample, before incubation with the detection antibody cocktail (2 h at room temperature). Immunoreactivity was detected by chemiluminescence using X-ray film (Fuji Medical) to visualize the dots. Images were analysed with the ImageJ open-source image software (<https://imagej.nih.gov/ij/>). Data were corrected for the local background and normalized for positive and negative internal controls.

2.11 | Study approval

All animal procedures were approved and performed according to the guidelines set out by the Institutional Ethics Committee for Animal Experimentation (protocol No 15005AE/07/FUN01/FIS02/JACP1).

3 | RESULTS

3.1 | Generation of NSC with the capacity to generate GBM in vivo

In keeping with our previous report (Almengló et al., 2017), both LP- and HP-immortalized cultures obtained from mouse embryo brains retain their capacity to express specific markers for all neural lineages (data not shown). Also in concordance with our previous findings, neurosphere formation can be induced by placing the cells under NBE conditions (data not shown). Altogether, these characteristics indicate that both types of cultures can be considered as bona fide immortalized NSC.

In addition, we also reported previously that HP-immortalized NSC show a sharp increase in their proliferative rate, as compared with either primary or LP-immortalized cells, together with the presence of numeral chromosomal abnormalities (Almengló et al., 2017). As these phenotypical traits may indicate a potential for cellular transformation, in the present study, we first investigated their capacity to generate brain tumours in vivo. To this end, cell suspensions of either LP- or HP-immortalized NSC were injected into the cerebral parenchyma of C57BL/6 mice. As Table 1 shows, development of orthotopic tumours was observed in all mice injected with HP-immortalized NSC (40, 60, or 90 passages), as soon as 3.5 months of injection (see also Figure 2a). In contrast, no tumours were observed in mice injected with either primary cultures or LP (15 passages) immortalized cells. The tumours showed many of the distinctive characteristics of GBM (Louis et al., 2016) including an infiltrative growth pattern, marked cellular pleomorphism, and the presence of regions of necrosis. Extensive vascular hyperplasia, thrombus formation, and invasion of vessel walls, together with prominent Ki67 expression (Figure 2b,d) were also present. In contrast, neither GFAP nor MBP expression was detected (Figure 2c), a finding in keeping with previous reports indicating that GBM typically displays loss of glial marker expression, including GFAP (Louis et al., 2016). Demonstration that tumours are not spontaneously generated but arise from the injected cells was obtained by detecting the expression of RFP in the tumour cells (Figure 2e).

To further characterize the generated tumours, we investigated their ability to retain bona fide NSC features in vitro. As occurs with immortalized NSC, cells isolated from GBM can grow as a monolayer culture, that can be induced to form neurospheres by placing them in NBE conditions (Figure 3a,b). Also, in keeping with the results

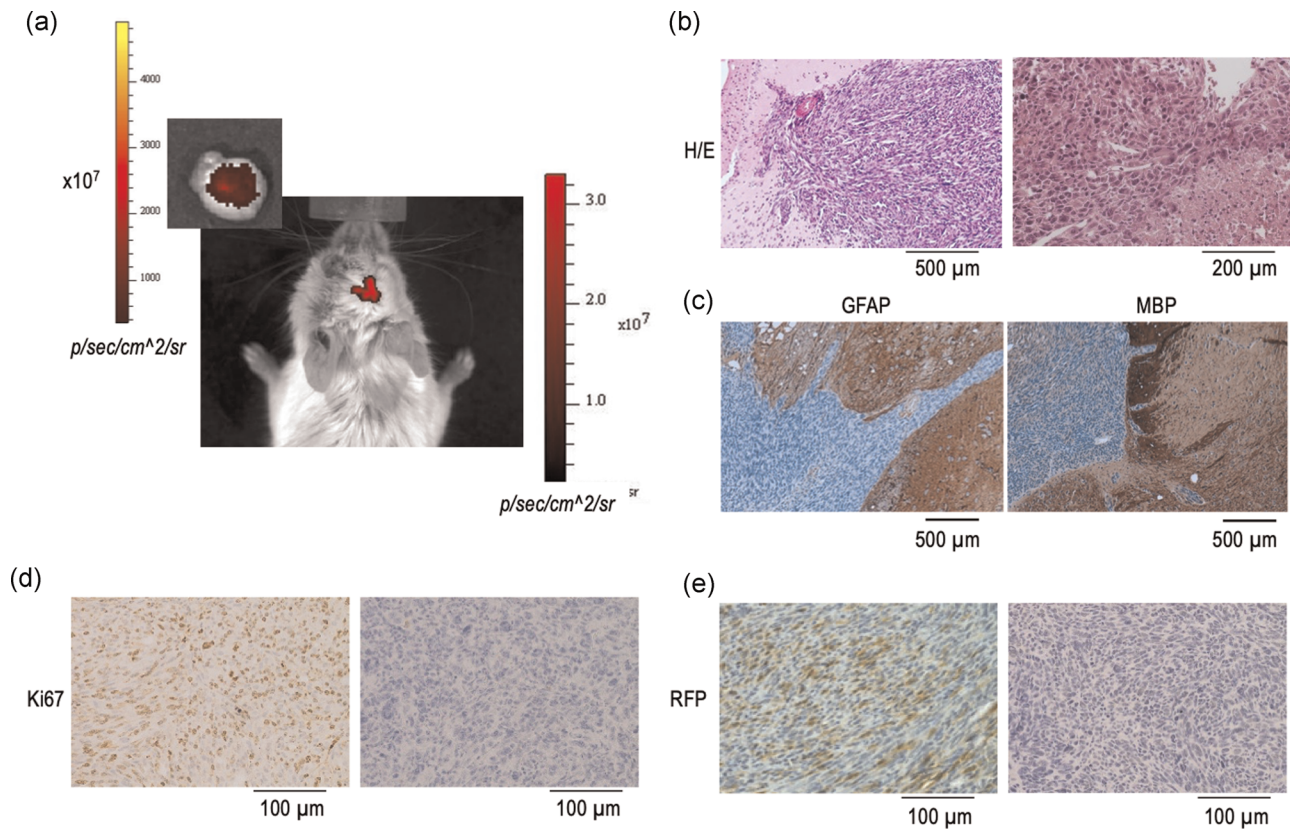


FIGURE 2 Generation of GBM in mice after orthotopic injection of high-passage-immortalized NSC. Cell suspensions of 3×10^5 cells obtained from primary cultures, low-passage-immortalized NSC (15 passages) or high-passage-immortalized NSC (40, 60, or 90 passages) were injected into the brain of C57BL/6 mice. (A) In vivo fluorescence imaging of one tumour generated 3.5 months after the injection. A more detailed ex vivo image of the brain is shown in the insert. (B) Representative haematoxylin-eosin staining showing some of the pathological hallmarks of GBM, including the marked cellular pleomorphism, and the presence of regions of extensive vascular hyperplasia, vascular invasion, and necrosis. (C) Immunohistochemical staining showing the absence of either GFAP or MBP expression in tumour cells, as compared with the prominent expression of both markers in the nearby normal brain. (D) Immunohistochemical detection of Ki67 shows increased expression in GBM (left), as compared with negative controls (right). (E) Demonstration that GBM arise from injected cells was obtained by immunohistochemical detection of the RFP protein (left), while no RFP expression was detected in negative controls (right). GBM, glial fibrillary acidic protein; MBP, myelin basic protein; NSC, neural stem cell; RFP, red fluorescent protein.

obtained in immortalized NSC, GBM-derived cells retain their capacity to express specific markers from all three neural lineages (Figure 3b,c), although a prominent decrease in GFAP expression was observed in this case. As expected, GBM-derived cells are also capable of inducing the formation of GBM in mice after orthotopic injection (Figure 3d,e), which can be detected in vivo as soon as 1 month after the injection. Histological and immunohistochemical analysis of these GBM were almost identical to those of the tumours generated after orthotopic injection of HP-NSC, including the lack of expression of both GFAP and MBP (data not shown).

3.2 | Generation of NSC with the capacity to generate heterotopic (metastatic) tumours in vivo

One of the more intriguing aspects of the biology of GBM is their ability to form metastasis, most likely because of the notion that extracranial/extraspinal metastases of human GBM are clinically rare (Awan et al.,

2015; Goodwin et al., 2016; Hoffman et al., 2017; Taskapilioglu et al., 2013). Therefore, we took advantage of our cellular model to investigate the ability of either HP-immortalized NSC or GBM-derived cells to form metastatic (heterotopic) tumours in vivo after injection in the tail vein of C57BL/6 mice. As Table 2 shows, macroscopic lung tumours were observed in all mice injected with HP-immortalized NSC (four mice) after 6 months of injection. In contrast, no tumours were detected after 3 or 4 months of injection of HP-immortalized NSC. In addition, a macroscopic lung tumour was also detected in one of three mice injected with GBM-derived cells, although, in this case, the tumour developed as soon as 3 months after injection (Table 2 and Figure 4a). Macroscopic examination of metastatic lungs showed the presence of single or multiple metastatic nodules with cannonball appearance and frequent haemorrhagic foci (Figure 4b), which was more clearly evidenced after low magnification of haematoxylin and eosin staining of the lung (Figure 4c). Microscopic examination of the tumours showed the distinct characteristics of GBM-derived cells when analyzed at higher magnification. These include the presence of marked cellular pleomorphism and necrosis

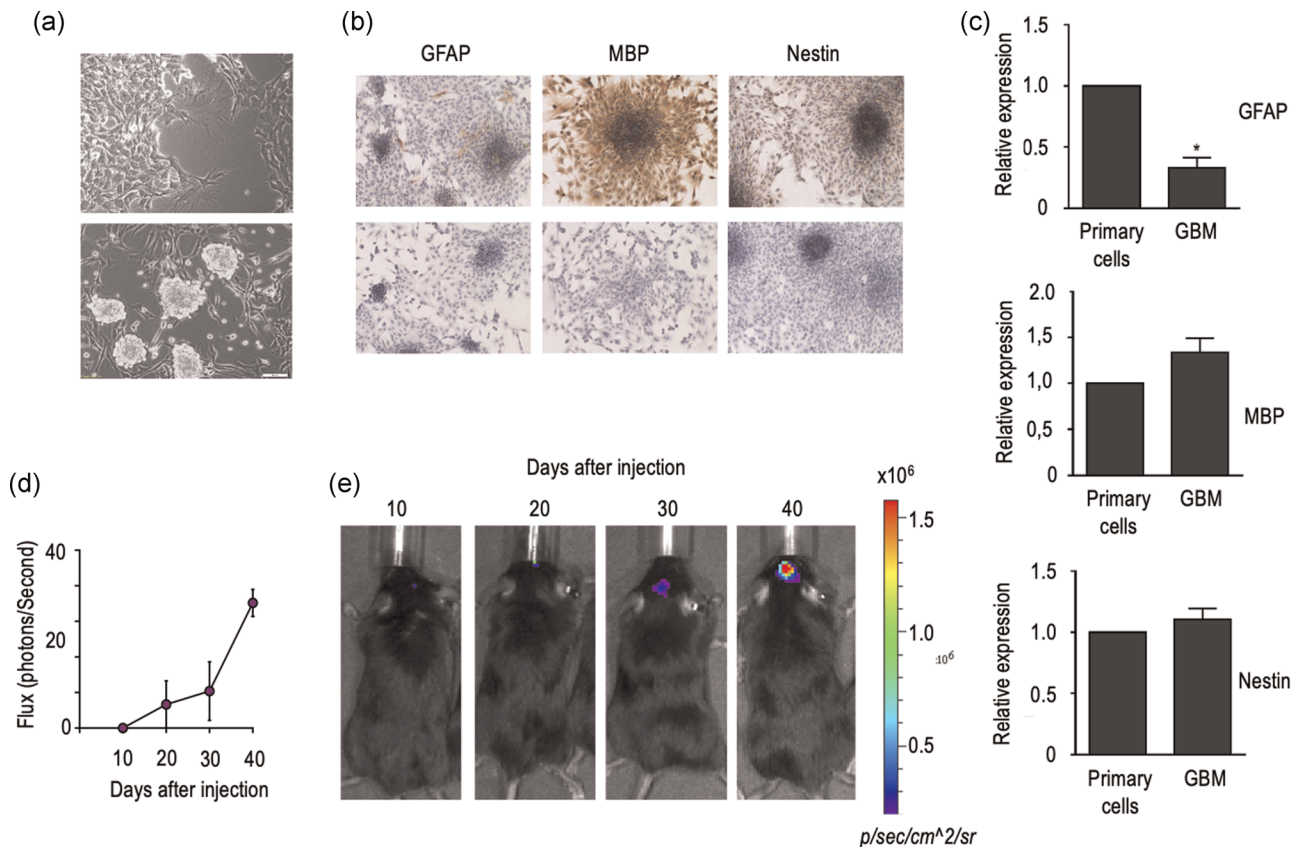


FIGURE 3 Cells derived from GBM retain NSC characteristics. GBM were dissociated and cells were grown in DMEM (see materials and methods for further details). Neurosphere formation was induced by placing the cells in NBE conditions. (A) Neurosphere formation was induced by placing the cells in NBE conditions. (B) Expression of specific markers of neural lineage (GFAP, MBP, and nestin) was detected by immunocytochemistry (lower panels are the negative controls). (C) Expression of specific neural markers was also demonstrated by semiquantitative RT-PCR (in this case, primary cells were used as control). (D, E) Real-time bioluminescent imaging of the tumoral growth in vivo, after orthotopic injection of GBM-derived cells. Results in (D) are the mean \pm SEM of six animals. Representative images are shown in (E). DMEM,; GBM,; NBE,; NSC,; RT-PCR,;

(Figure 4d), together with the existence of prominent Ki67 expression (Figure 4e). As in the case of primary brain tumours, neither GFAP nor MBP expression was detected in tumoural cells (Figure 4f). Also in this case, a demonstration that metastatic (heterotopic) tumours arise from injected cells was obtained by investigating the existence of RFP expression (Figure 4g). Furthermore, cells isolated from metastatic tumours can grow as monolayer cultures that can be induced to form neurospheres when placed in NBE conditions (Figure 5a). As also occurs with GBM-derived cells, cells obtained from heterotopic tumours retained the expression of specific markers for all neural lineages (Figure 5a and b), with a sharp decrease in the case of GFAP (Figure 5b).

Despite the low rate of extracranial metastasis that exists in GBM, recent reports have described the existence of circulating tumour cells (CTC) in the peripheral blood of patients with GBM (Awan et al., 2015; Li et al., 2017; Seoane & De Mattos-Arruda, 2014). Therefore, to further investigate the blood dissemination of the injected cells, we performed cellular cultures of the brain, kidney, spleen, bone marrow, testicles, and liver, obtained from mice injected with either HP-immortalized cells or GBM-derived cells. In all cases, the presence of tumoral cells in these tissues was demonstrated by growing primary

cultures in DMEM, and inducing the formation of neurospheres by placing them in NBE conditions. Although macroscopic tumours were not detected in any of those organs, formation of neurospheres and, therefore, evidence of the existence of microscopic heterotopic tumours was found in the kidney (Figure 6), liver, and spleen (Table 2). In addition, lung microscopic metastasis were also found in two mice with the absence of macroscopic lung tumours (Table 2). In contrast, generation of neurospheres was not observed, in any case, in primary cultures from bone marrow, testicle, or brain. As expected, neurospheres expressed specific markers for all neural lineages, though GFAP expression was also sharply reduced in this case (Figure S1).

3.3 | Phenotypical characterization of immortalized, tumoral and metastatic NSC

Altogether, our results demonstrate that continual passaging of cell cultures obtained from mouse embryo brain results in the generation of immortal cells with NSC characteristics that, finally, acquire the capacity to generate both primary GBM and heterotopic tumours in

TABLE 2 Generation of metastatic tumours in mice after IV injection of high-passage-immortalized NSC (cell type 3) or GBM-derived cells (cell type 4) (see Figure 7 for further details)

Mice No.	Cell type (passages)	Time to tumour (months)	Organ
1	3 (40)	4	No tumour
2	3 (40)	4	No tumour
3	3 (40)	6	Lung, kidney,* spleen*
4	3 (40)	6	Lung
5	3 (60)	4	No tumour
6	3 (60)	4	No tumour
7	3 (60)	4	No tumour
8	3 (90)	3	No tumour
9	3 (90)	4	No tumour
10	3 (90)	6	Lung, kidney*
11	3 (90)	6	Lung, liver*
12	4	3	Lung,* liver*
13	4	3	Lung
14	4	3	Lung,* liver*

Note: *denote the presence of microscopic tumours.

vivo. Therefore, to better understand the mechanisms underlying this transformation, we next investigated the presence of cellular aneuploidy, one of the hallmarks of the oncogenic process (Duesberg et al., 1998; Li et al., 1997; Rasnick & Duesberg, 1999). As Figure 6 depicts, more than 80% of primary cells have 40 chromosomes, but a sharp increase in the number of numerical chromosome abnormalities is observed in immortalized cells, even in LP cells. This finding is in concordance with our previous reports (Almengló et al., 2020) and indicates that hyperploidy is an early event within the transformation process of NSC. Although the percent of cells with severe polyploidy is greater in HP-immortalized or in tumoral (either primary or heterotopic) cells, the most striking changes occur soon after immortalization is achieved.

These changes in cellular aneuploidy correlate with other phenotypical and biochemical modifications observed. When compared with primary cells, both LP- and HP-immortalized cells showed an increase in their proliferation rate (Figure 7a,b), a finding that is also in keeping with our previous results (Almengló et al., 2020). Interestingly, the increase in growth rate observed in HP-immortalized cells is similar to that observed in GBM-derived cells (Figure 7a,b), and contact inhibition was preserved in both cases (data not shown). However, the highest proliferative rate was observed in cells obtained from heterotopic tumours, either generated from HP-immortalized cells or GBM-derived cells (Figure 7a,b). These differences in cell proliferation sharply correlate with the changes

observed in the expression of Ki67 and in the rate of BrdU incorporation. In fact, while <50% of either primary or LP-immortalized cells show immunoreactivity to Ki67, more than 90% of HP-immortalized or GBM-derived cells, and virtually all cells derived from heterotopic tumours are Ki67+ (Figure 7c). In the case of BrdU incorporation, a significant increase was already observed in LP-immortalized cells when compared with control cells, but the most striking boost was found in HP-immortalized NSC. BrdU uptake remained similarly increased among all tumour-derived cell types, either primary or metastatic (Figure 7d). Also in keeping with our previous findings, continual cell passaging resulted in the appearance of dramatic morphological changes. Although flat, polygonal cells were still present in hastily growing cells, most of them displayed distinct morphological modifications, including the presence of multinucleated cells with very large cytoplasm and long thin projections (data not shown).

3.4 | Biochemical characterization of immortalized, tumoral and metastatic NSC

Finally, we investigated the biochemical changes underlying the timeline of the modifications that led to the transformation of primary cells into GBM-producing cells. Although GBM displays a heterogeneous profile, a common feature of all GBM types is an aberrant kinase signalling, and among the pathways implicated, the RAS-mitogen-activated protein kinase (MAPK), is one of the most frequently dysregulated in GBM cells (Hannen et al., 2017; Lo, 2010; Mao et al., 2012). In keeping with this, undetectable levels of either Raf-1 or ERK1 phosphorylation were observed in both primary cultures and LP-immortalized cells (Figure 8a), while a clear rise was detected in HP-immortalized cells. Furthermore, this activation was progressively increasing throughout the transformation process, with the highest phosphorylation levels found in cells from heterotopic tumours. A similar pattern of activation was observed in the case of the two leading members of the RSK (90 kDa ribosomal S6 kinase) family, RSK1 and RSK2, two downstream effectors of the ERK pathway (Romeo et al., 2012) (Figure 8a). RSK1 phosphorylation was undetectable in either primary or LP-immortalized cells, but progressively increased in the other cell types, with the highest phosphorylation levels detected in cells from heterotopic tumours. In the case of RSK2, no phosphorylation was detected in primary, LP-immortalized, and HP-immortalized cells, and phosphorylation levels were also unexpectedly low in cells from heterotopic tumours originated from HP-immortalized NSC. Interestingly, although both RSK1 and RSK2 are associated with glioma malignancy, RSK1 has been described as a potential progression marker and a therapeutic target for gliomas. In fact, RSK1 phosphorylation levels (Ser380), which more specifically reveals ERK activation, are higher in GBM (Hajj et al., 2020). Additionally, RSK1 phosphorylates p27 at Thr198, leading to accumulation of phosphorylated p27 in the cytoplasm (Larrea et al., 2009). Accordingly, p27 levels progressively increased with a similar pattern to that observed in RSK-1. These findings,

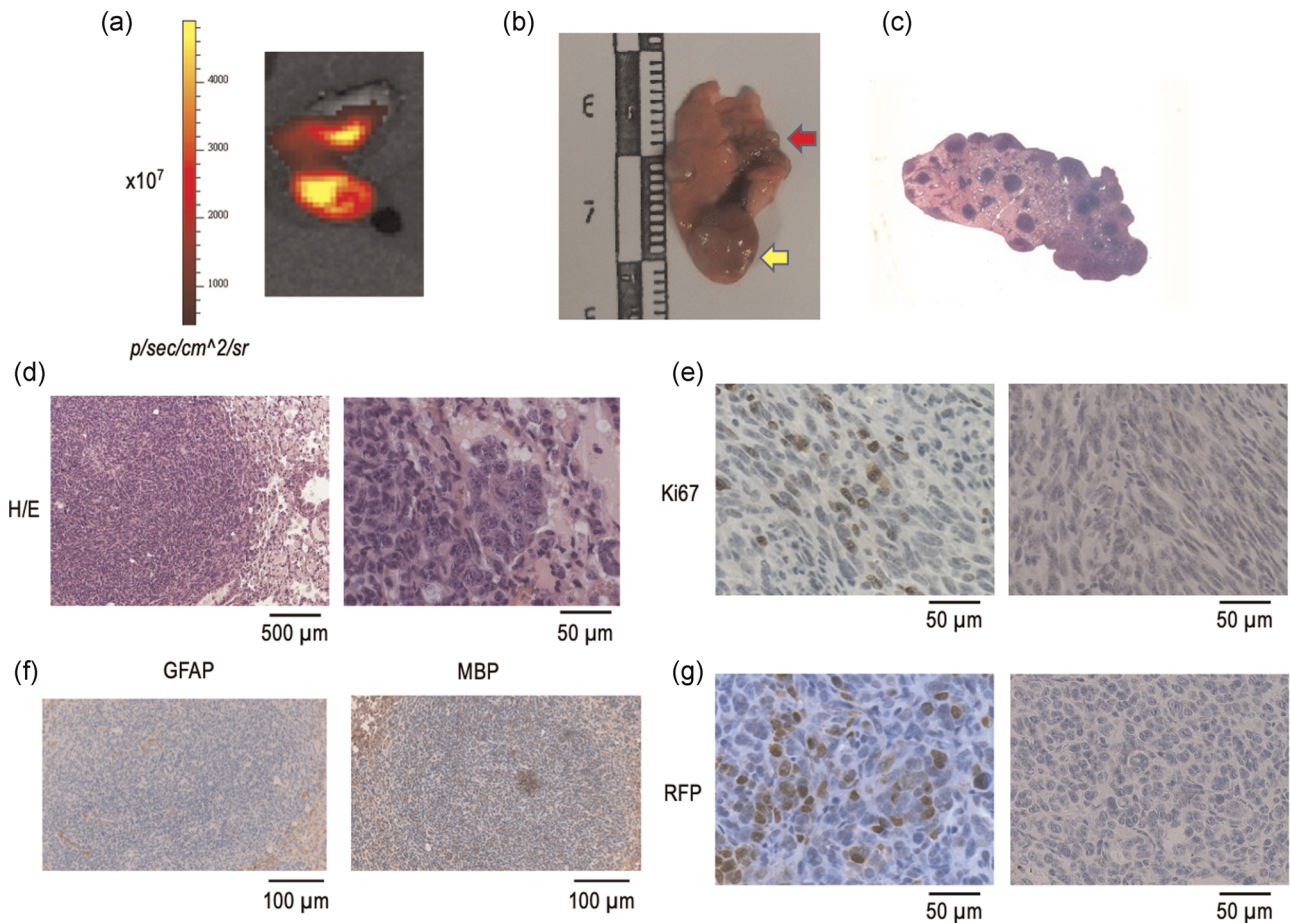


FIGURE 4 Generation of metastatic lung tumours in mice after heterotopic injection of high-passage-immortalized or GBM-derived cells. Cell suspensions of 3×10^5 cells obtained from either high-passage-immortalized NSC (90 passages) or GBM-derived cells were injected in the tail vein C57BL/6 mice. (A) Ex vivo fluorescence imaging of a metastatic lung after 6 months of heterotopic cell injection. (B) Macroscopic aspect of one representative metastatic lung. Notice the presence of cannonball-like tumours (yellow arrows), together with the existence of haemorrhagic areas (red arrows). (C) Low magnification image of an entire haematoxylin-eosin stained section revealing the presence of multiple metastasis. (D) Haematoxylin-eosin staining reveals the presence of blood vessels surrounding the micro metastases in addition to the tumour's own vasculature. (E) Immunohistochemical detection of Ki67 shows increased expression in the tumour (left), as compared with the negative control (right). (F) Immunohistochemical staining showing the absence of either GFAP or MBP expression in tumour cells. (G) Demonstration that GBM arise from injected cells was obtained by immunohistochemical detection of the RFP protein (left), while no RFP expression was detected in the negative control. GBM,; NSC,; RFP,;

together with the increased levels of p53 detected, may suggest that, as we have previously shown (Seoane et al., 2017), increased cell proliferation (and, eventually, cell transformation) may occur despite the existence of a normal activation of the cellular checkpoints involved in the induction of senescence. Surprisingly, a so clear pattern of activation was not observed when other signalling pathways were investigating. This is the case of the phosphatidylinositol 3-kinase (PI3K)-Akt pathway that is activated in almost 90% of all GBM (Li et al., 2016; Sami & Karsy, 2013; Sanai et al., 2004). However, we were unable to find any difference in the phosphorylation level of the leading members of this pathway, including PI3K, Akt, phosphatase and tensin homolog (PTEN) or mammalian Target of rapamycin (mTOR) (Figure S2), among the different cell types. Overall, these results indicate that immortalization of NSC may be associated with a progressive activation of the Ras/Raf/ERK signalling pathway.

4 | DISCUSSION

In the present study, we have demonstrated that continual passaging of immortalized NSC results in their transformation into cells that are able to produce either GBM or heterotopic tumours, when injected in adult mice. Although further studies are still necessary, our results support a role for NSC in the pathogenesis of GBM, at least for primary GBM, which accounts for more than 90% of this type of tumours (Joshi et al., 2015). This proposal is in keeping with other studies indicating that NSC may be the cells from which GBM originate, due to their self-renewal and proliferative capacities, and the relevance of the accumulation of somatic mutations in the process of gliomagenesis (Alcantara Llaguno et al., 2009; Batlle & Clevers, 2017; Richards et al., 2021; Sanai et al., 2004).

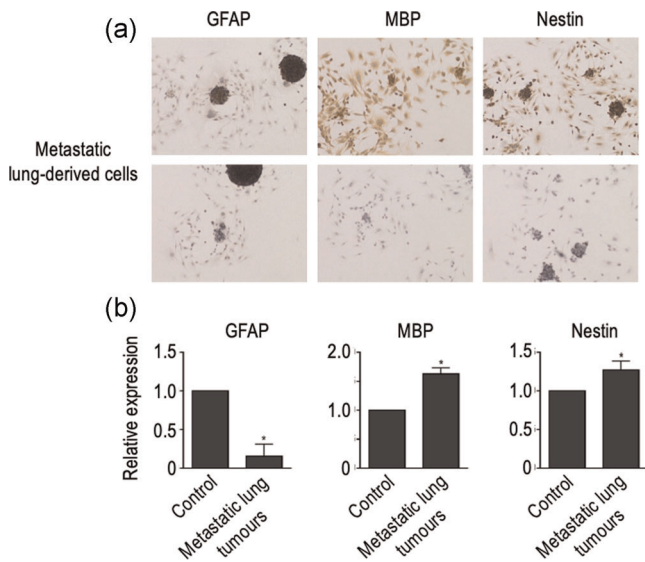


FIGURE 5 Cells derived from lung metastatic tumours display NSC characteristics. Lung tumours were dissociated, and cells were grown in DMEM (see materials and methods for further details). (A) Neurosphere formation was induced by placing the cells in NBE conditions. Expression of specific markers of neural lineage (GFAP, MBP, and nestin) was detected by immunocytochemistry in cells derived from metastatic lung tumours. Lower panels are the negative controls. Notice the presence of neurospheres attached to the culture dish in all cases. (B) Expression of specific neural markers was also demonstrated by semiquantitative RT-PCR (in this case, primary cells were used as control). Notice the reduced expression of GFAP, as observed in GBM. DMEM.; GBM.; GFAP, glial fibrillary acidic protein; MBP, myelin basic protein; NSC.; RT-PCR;

The role of embryonic stem cells in cancer has been largely debated. Cancer initiating cells or cancer stem cells (CSC) are a subpopulation of cells that has the driving force of carcinogenesis (Alcantara Llaguno et al., 2009; Battle & Clevers, 2017) that can be identified in most types of human cancer (Bonnet & Dick, 1997; Chang, 2016; Smith et al., 2008; Tomasetti et al., 2017). Although not all CSC are originated from embryonic cells, specific criteria to define CSC include (1) the ability to self-renew; (2) the capacity to differentiate into different lineages (multipotency); and (3) the ability to initiate tumours in animal models, which recapitulate the original disease phenotype and heterogeneity (Doherty et al., 2016; Sawada & Sawamoto, 2013; Singh et al., 2004; Takaishi et al., 2009). All these criteria are fulfilled by the HP-immortalized NSC used in this study and, therefore, they can be considered as truly CSC, thus supporting the hypothesis of NSC as the source of GBM. In this regard, it has been recently demonstrated that astrocyte-like NSC in the SVZ are the cell of origin that contains the driver mutations of human GBM (Lee et al., 2018). Furthermore, astrocyte-like NSC that carry driver mutations migrate from the SVZ and lead to the development of high-grade malignant gliomas in distant brain regions (Lee et al., 2018).

Of special interest is the fact that no “external” hit is needed to induce the malignant transformation of NSC, other than their

continuous passaging and the stress induced to overcome replicative senescence (Almengló et al., 2020). In fact, in contrast with the results reported in MEF placed on a 3T3 protocol, in which immortal cells emerge at low frequency (Todaro & Green, 1963), we were able to generate immortal NSC with a 100% frequency. Furthermore, all HP-immortalized NSC were able to generate GBM when orthotopically injected in mice. Therefore, it is tempting to speculate that the mechanisms that allow primary cells to escape from replicative senescence are those leading to malignant transformation. In this context, it is interesting to note that those NSC that can overcome replicative senescence show increased activation of both p27 and p53 (Almengló et al., 2020, and the present work). This result, together with the early occurrence of hyperploidy in immortalized NSC may suggest the existence of an uncoupled response to the activation of the DNA damage response (DDR). Interestingly, similar results have been previously reported by our group in response to oncogene-induced senescence (OIS) in primary MEA (Seoane et al., 2017). In those cells, activation of Ras and elimination of RB does not induce cellular senescence, despite the activation of the cellular checkpoints related to DDR. It must be emphasized that MEA are the cells that give rise to immortal NSC after overcoming replicative senescence (Almengló et al., 2017, 2020, and the present study). Therefore, the ability of MEA to escape cellular senescence, either replicative or OIS, could underlie an important role in gliomagenesis.

Although we do not presently know the mechanisms involved in this defective response, it is interesting to notice that the transition from primary to immortalized cells is associated with an almost total loss of euploid cells. Aneuploidy is one of the hallmarks of most human cancers, with around 90% of all solid tumours being aneuploid, mostly hyperdiploid (Coward & Harding, 2014; Duensing & Duensing, 2010; Weaver & Cleveland, 2008). Although both the mechanisms leading to aneuploidy and their consequences on tumorigenesis are still controversial, it has been proposed that tumour cells with significantly elevated genomic content (polyploid tumour cells) facilitate rapid tumour evolution. Furthermore, aneuploidy has been shown to precede transformation in a variety of cancers (Cardoso et al., 2006; Doak et al., 2004; Dooley et al., 1993; Ried et al., 1999), and it has been proposed a role of aneuploidy during tumour initiation (Duesberg et al., 1998; Li et al., 1997). In keeping with this, severe polyploidy was also an early event in the natural history of the transformation process described in the study, so it can be hypothesized that it may be involved in the appearance of the other biochemical and phenotypical changes observed, including the increased activation of ERK signalling (Furgason et al., 2014; Jun et al., 2018).

It remains to be elucidated whether similar mechanisms may account for the oncogenic transformation of NSC in vivo. Under physiological conditions, NSC are regulated by the orchestration of intrinsic and extrinsic signals that provide the complex regulatory architectures present in the neurogenic niche. The special micro-environment defined within the neurogenic niche permits the maintenance of the NSC pool and prevents terminal differentiation, thus allowing the balance between cell loss and cell replacement in

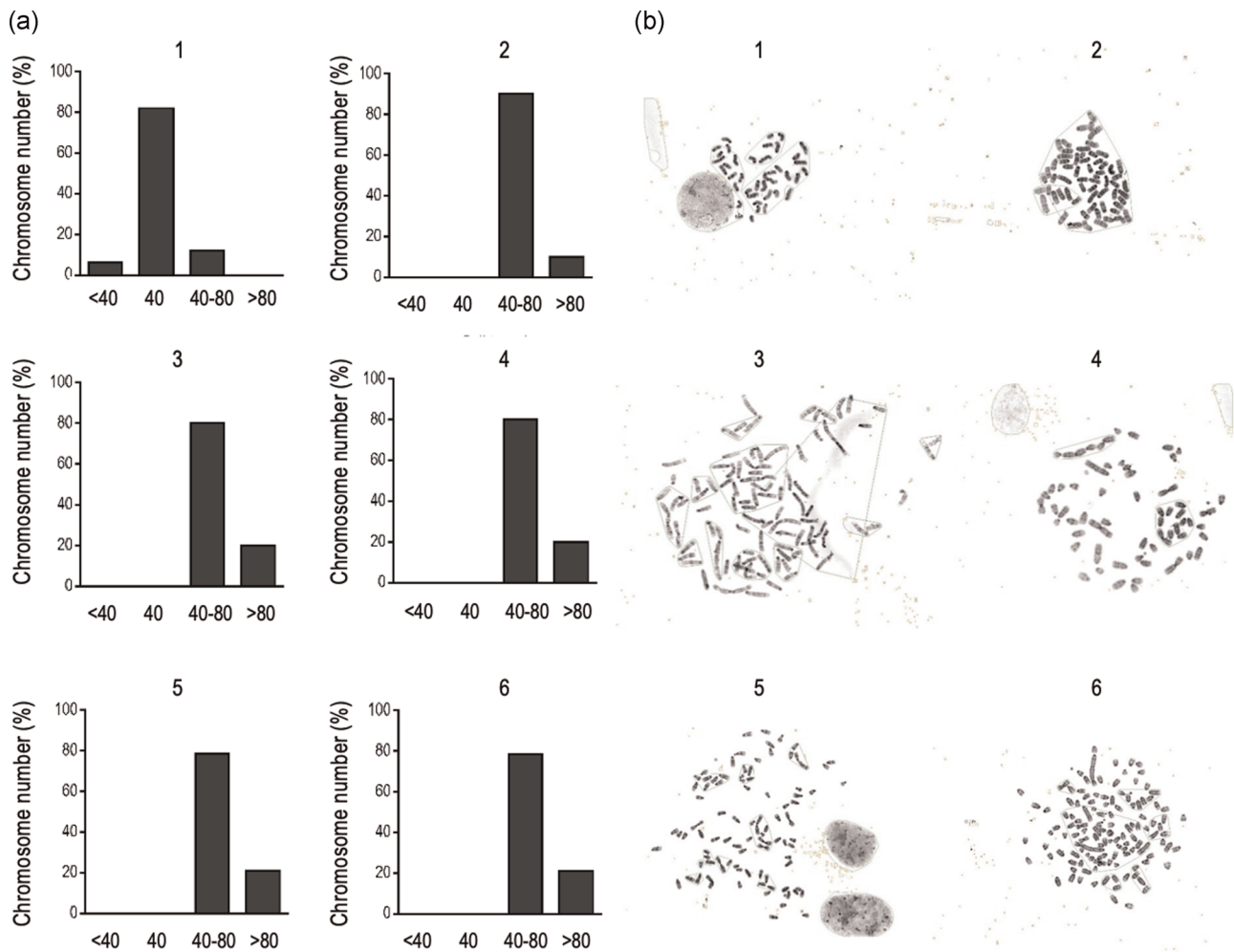


FIGURE 6 Numerical chromosome abnormalities increase throughout the transformation process. Metaphase spreads were prepared from primary (1), low-passage-immortalized (2), high-passage-immortalized (3), GBM-derived (4), and metastasis-derived (5 and 6) cells. In all cases, cells were spotted onto microscope slides and stained with 2% Wright in Gurr buffer (pH 7.0), and metaphase chromosomes were scored using a Leica 2005 microscope under a 100X oil objective lens. (A) Distribution of chromosome number (percent) for each cell type. A dramatic increase in the number of hyperploidy cells is already present in low-passage-immortalized cells and maintained in the other cell types. (B) Representative images of results presented in (A)

the central nervous system (Arce et al., 2013; Gage, 2000; Vining & Mooney, 2017). Under our experimental conditions, cells are grown in the presence of FBS and, therefore, exposed, for a long time, to a wealth of growth factors that are not present within the neurogenic niche. Therefore, it is tempting to speculate that disturbance of the microenvironment within the neurogenic niche may result in a dys-regulated proliferation of NSC that, eventually, may cause the appearance of a GBM. In this respect, it has been shown that NSC niches of the human brain may be a mutational source for brain somatic mutations (Coward & Harding, 2014). Furthermore, a recent report (Richards et al., 2021) directly links the healing process that follows a brain injury with the spur of GBM, when new cells generated to replace those lost to the injury are derailed by mutations.

Another interesting conclusion of this study is the capacity of immortalized NSC to disseminate and form heterotopic tumours when injected in mice. Extracranial/extraspinal metastasis is a very uncommon

entity in GBM, and only a low number of patients develop extracranial metastasis (Awan et al., 2015; Goodwin et al., 2016; Hoffman et al., 2017; Taskapiloglu et al., 2013). Although, historically, GBM were not believed to metastasize because of the presence of the blood-brain barrier, improvements in the treatment of primary GBM has led to an increased in reported metastasis, mostly in the lungs, but also in other organs such as lymphatic nodes, bone, or liver (Awan et al., 2015; Goodwin et al., 2016; Hoffman et al., 2017; Taskapiloglu et al., 2013). In keeping with this, we found that lungs were the organs that more frequently presented heterotopic tumours (macroscopic and microscopic), but a widespread hematogenous dissemination was observed. This capacity for hematogenous dissemination is in concordance with recent studies demonstrating the existence of CTC in the blood of 20%–39% of patients with GBM (Lombard et al., 2015; Sullivan et al., 2014). As occurrence of extracranial/extraspinal metastasis is expected to increase as GBM treatment becomes more efficient, our results support the validity of our model to

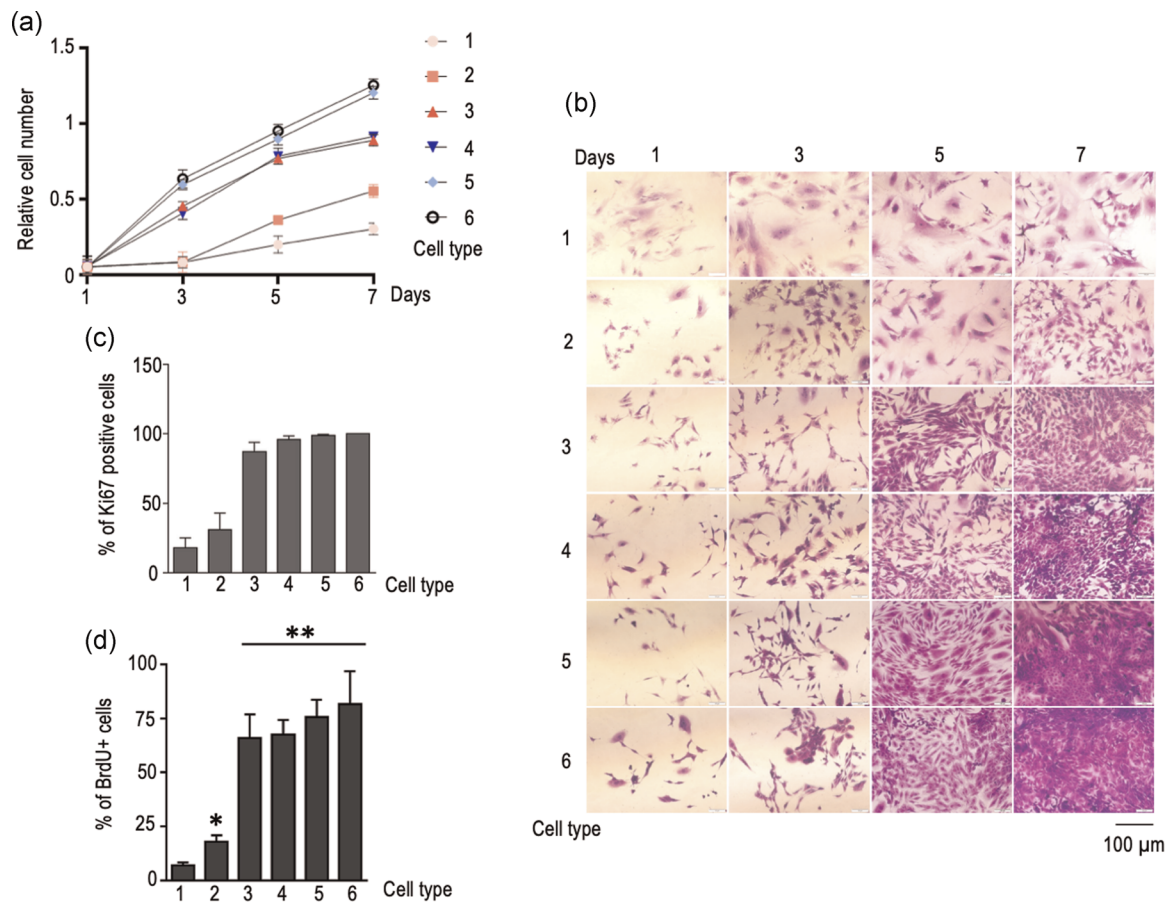


FIGURE 7 Cell proliferation progressively increases throughout the transformation process. (A) Primary (1), low-passage-immortalized (2), high-passage-immortalized (3), GBM-derived (4), and metastasis-derived (5 and 6) cells were cultured, and cell number was determined by crystal-violet staining. A progressive increase in the growth rate was observed from 1 to 5–6. (B) Representative images of results presented in panel A. (C) Ki67 staining in the different cell types. The percent of Ki67+ cells was determined after scoring them by immunocytochemistry. (D) BrdU incorporation was determined by immunocytochemistry. In this case, each bar represents the mean + SEM of three experiments in triplicate. * $p < .05$ versus primary cells. BrdU; GBM,;

mimic in vitro the natural course of the disease in vivo. It is also quite remarkable that HP-immortalized NSC have the same capacity to be highly metastatic as cells obtained from primary GBM. This indicates that metastatic genotype is acquired early in tumour progression as has been already proposed (Bernards & Weinberg, 2002; van de Wouw et al., 2002).

In summary, we have developed an experimental model that allows recapitulating the process of transformation of mouse embryo NSC into GBM-producing cells in vitro. As most of the cells enter in senescence when submitted to the 3T3 protocol (Almengló et al., 2020, and the present study), we do not presently know whether all the SC present in the culture or just a fraction of them are able to overcome senescence. In other words, it remains to be elucidated whether all NSC have the capacity of immortalization, or only some of them, because of a transformation process. In any case, we have found that the transformation process occurs with a 100% frequency, thus suggesting that oncogenic transformation is the unavoidable fate for, at least, a population of NSC when undergoing long-term proliferation in vitro. Furthermore, the transformation likely occurs because of the presence of serum factors in

the culture medium, thus highlighting the importance of maintaining the NSC in an adequate environment. While it remains to be elucidated whether a similar mechanism may be involved in the pathogenesis of GBM in vivo, a warning should be made about the transplantation of NSC as a tool for neural repair (Arce et al., 2013).

Finally, we also describe a novel model of gliomagenesis that recapitulates in vitro the transformation of primary MEA into cells that are able to generate both GBM and heterotopic tumours in vivo (Figure 8b). This model has two important advantages over current systems. First, it can be used to recapitulate the pathogenesis of GBM and, therefore, to elucidate the timeline of the mutations that accounts for the generation of GBM. Second, it provides us with a valuable tool to test the effectiveness of therapeutics at different times throughout the natural history of the disease. This characteristic would help the development of personalized treatment strategies by tailoring drug effectiveness with mutational profiles. Finally, given the ability of all cell types (including those derived from GBM or heterotopic tumours) to form neurospheres when placed on NBE conditions, they can be used to generate 3D organoid culture systems (Kadoshima et al., 2013; Paşca et al., 2015) to capture

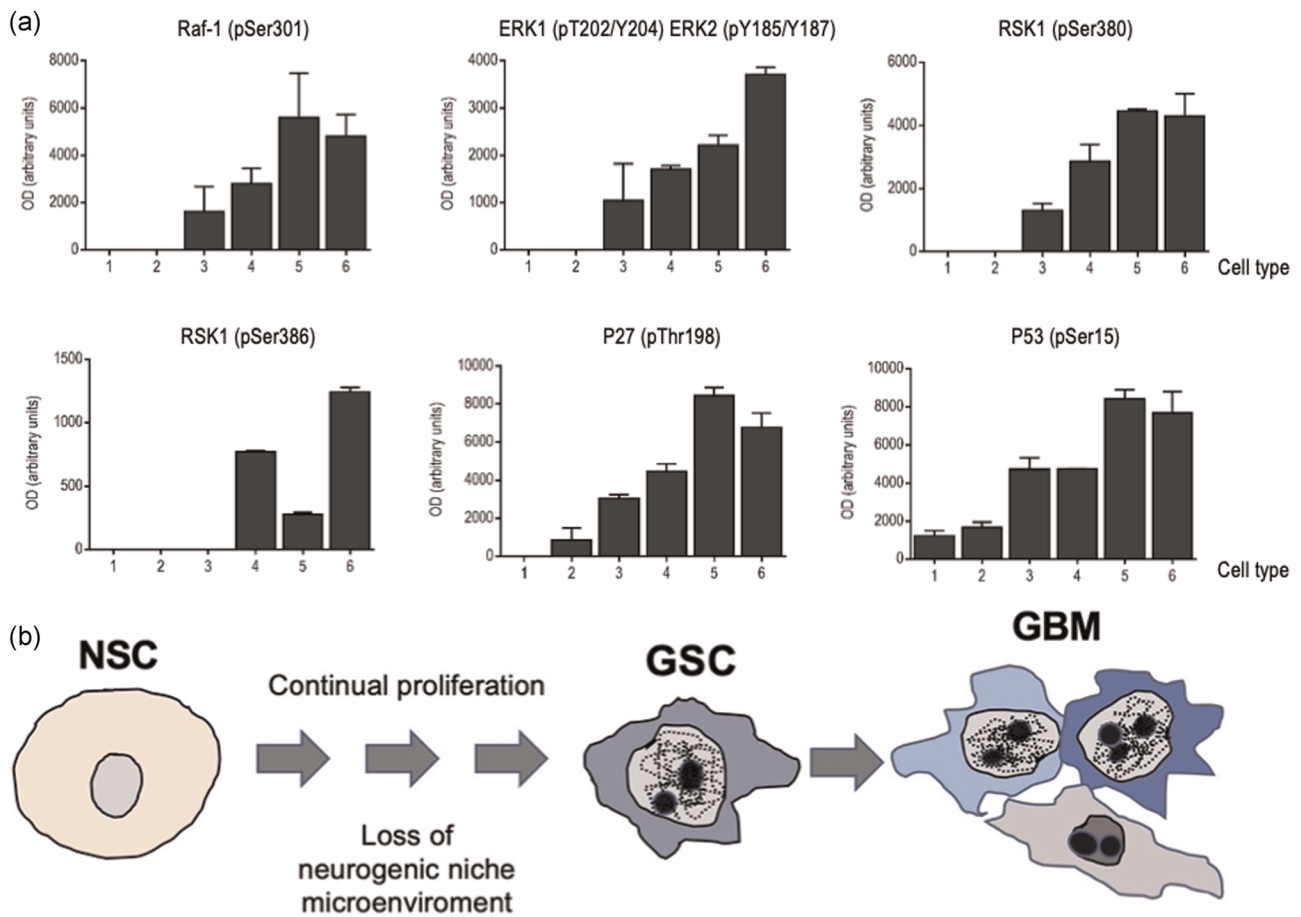


FIGURE 8 Transformation of immortalized NSC. (A) An increase in the activation of the ERK signalling pathway is associated with transformation. Primary (1), low-passage-immortalized (2), high-passage-immortalized (3), GBM-derived (4), and metastasis-derived (5 and 6) cells were cultured and the phosphorylation levels of proteins of the Ras-Raf-ERK pathway (Raf-1, ERK1, RSK1, RSK2), p27 and p53 were investigated. A progressive increase in the activation of the pathway was observed throughout the process, with the highest lowest phosphorylation levels found in primary or low-passage-immortalized cells (cell types 1 and 2, respectively) and the highest levels in cells obtained in cells from heterotopic tumours (cell types 5 and 6). (B) Schematic representation of the transformation process. GBM; NSC;

the phenotypic and molecular particularities of GBM, as we have recently shown (Gomez-Randulfe et al., 2019).

ACKNOWLEDGMENTS

We acknowledge C. Watzl (Institute for Immunology, University Heidelberg) for providing us with the Phoenix-Eco packaging cells. The expert technical help of Ana Senra is also greatly acknowledged. This study was supported in part by Xunta de Galicia (2014-PG029), University of Santiago de Compostela (2018-PU001), Ministerio de Economía y Competitividad (P115/01129, José A. Costoya), the Centro Singular de Investigación de Galicia accreditation 2016–2019, ED431G/05, and the European Regional Development Fund (ERDF).

CONFLICTS OF INTEREST

The authors declare no conflict of interest. @@@The founding sponsors had no role in the design of the study; in the collection, analyses, or interpretation of data; in the writing of the manuscript, and in the decision to publish the results.

AUTHOR CONTRIBUTIONS

Conceptualization: Cristina Almengló, José A. Costoya, and Víctor M. Arce. *Data curation:* Cristina Almengló, Máximo Fraga, Jesús Devesa, José A. Costoya, and Víctor M. Arce. *Formal analysis:* Cristina Almengló, Jesús Devesa, José A. Costoya, and Víctor M. Arce. *Funding acquisition:* José A. Costoya and Víctor M. Arce. *Investigation:* Cristina Almengló, Pilar Caamaño, Máximo Fraga, Jesús Devesa, José A. Costoya, and Víctor M. Arce. *Methodology:* Cristina Almengló, Pilar Caamaño, and Máximo Fraga. *Project administration:* José A. Costoya and Víctor M. Arce. *Supervision:* Jesús Devesa, José A. Costoya, and Víctor M. Arce. *Writing—review and editing:* Cristina Almengló, Jesús Devesa, José A. Costoya, and Víctor M. Arce.

DATA AVAILABILITY STATEMENT

All relevant information is presented within the article. Additional data that support the findings of this study are available from the corresponding author upon reasonable request.

ORCID

José A. Costoya  <http://orcid.org/0000-0003-3691-6419>

Victor M. Arce  <http://orcid.org/0000-0003-2391-6217>

REFERENCES

- Alcantara Llaguno, S., Chen, J., Kwon, C.-H., Jackson, E. L., Li, Y., Burns, D. K., Alvarez-Buylla, A., & Parada, L. F. (2009). Malignant astrocytomas originate from neural stem/progenitor cells in a somatic tumor suppressor mouse model. *Cancer Cell*, *15*, 45–56.
- Allen, M., Bjerke, M., Edlund, H., Nelander, S., & Westermarck, B. (2016). Origin of the U87MG glioma cell line: Good news and bad news. *Science Translational Medicine*, *8*(354), 354re3.
- Almengló, C., Devesa, P., Devesa, J., & Arce, V. M. (2017). GPE promotes the proliferation and migration of mouse embryonic neural stem cells and their progeny in vitro. *International Journal of Molecular Sciences*, *18*, 1280.
- Almengló, C., González-Mosquera, T., Caamaño, P., Seoane, M., Fraga, M., Devesa, J., Costoya, J. A., & Arce, V. M. (2020). immortalization of a cell line with neural stem cell characteristics derived from mouse embryo brain. *Developmental Dynamics*, *249*, 112–124.
- Arce, V. M., Devesa, P., & Devesa, J. (2013). Role of growth hormone (GH) in the treatment on neural diseases: From neuroprotection to neural repair. *Neuroscience Research*, *76*, 179–186.
- Awan, M. J., Liu, S. K., Sahgal, A., Das, S., Chao, S. T., Chang, E. L., Knisely, J., Redmond, K., Sohn, J. W., Machtay, M., Sloan, A. E., Mansur, D. B., Rogers, L. R., & Lo, S. S. (2015). Extra-CNS metastasis from glioblastoma: A rare clinical entity. *Expert Review of Anticancer Therapy*, *15*, 545–552.
- Azari, H., Sharififar, S., Rahman, M., Ansari, S., & Reynolds, B. A. (2011). Establishing embryonic mouse neural stem cell culture using the neurosphere assay. *Journal of Visualized Experiments*, *47*, 2457.
- Battle, E., & Clevers, H. (2017). Cancer stem cells revisited. *Nature Medicine*, *23*, 1124–1134.
- Bernards, R., & Weinberg, R. A. (2002). A progression puzzle. *Nature*, *418*, 823.
- Bonnet, D., & Dick, J. E. (1997). Human acute myeloid leukemia is organized as a hierarchy that originates from a primitive hematopoietic cell. *Nature Medicine*, *3*, 730–737.
- Caragher, S., Chalmers, A. J., & Gomez-Roman, N. (2019). Glioblastoma's next top model: Novel culture systems for brain cancer radiotherapy research. *Cancers*, *11*, 44.
- Cardoso, J., Molenaar, L., De Menezes, R. X., Van Leerdam, M., Rosenberg, C., Möslin, G., Sampson, J., Morreau, H., Boer, J. M., & Fodde, R. (2006). Chromosomal instability in MYH-and APC-mutant adenomatous polyps. *Cancer Research*, *66*, 2514–2519.
- Chang, J. C. (2016). Cancer stem cells role in tumor growth; recurrence; metastasis; and treatment resistance. *Medicine*, *95*(Suppl 1), S20–S25.
- Coward, J., & Harding, A. (2014). Size does matter: Why polyploid tumor cells are critical drug targets in the war on cancer. *Frontiers in Oncology*, *4*, 123.
- Doak, S. H., Jenkins, G. J., Parry, E. M., Griffiths, A. P., Baxter, J. N., & Parry, J. M. (2004). Differential expression of the MAD2; BUB1 and HSP27 genes in Barrett's oesophagus—Their association with aneuploidy and neoplastic progression. *Mutation Research/DNA Repair*, *547*, 133–144.
- Doherty, M. R., Smigiel, J. M., Junk, D. J., & Jackson, M. W. (2016). Cancer stem cell plasticity drives therapeutic resistance. *Cancers*, *8*, 8.
- Dooley, T. P., Mattern, V. L., Moore, C. M., Porter, P. A., Robinson, E. S., & Vandeberg, J. L. (1993). Cell lines derived from ultraviolet radiation-induced benign melanocytic nevi in Monodelphis domestica exhibit cytogenetic aneuploidy. *Cancer Genetics and Cytogenetics*, *71*, 55–66.
- Duensing, A., & Duensing, S. (2010). Centrosomes; polyploidy and cancer. *Advances in Experimental Medicine and Biology*, *676*, 93–103.
- Duesberg, P., Rausch, C., Rasnick, D., & Hehlmann, R. (1998). Genetic instability of cancer cells is proportional to their degree of aneuploidy. *Proceedings of the National Academy of Sciences of the United States of America*, *95*, 13692–13710.
- Furgason, J. M., Li, W., Milholland, B., Cross, E., Li, Y., McPherson, C. M., Warnick, R. E., Rixe, O., Stambrook, P. J., Vijg, J., & Bahassi, E. M. (2014). Whole genome sequencing of glioblastoma multiforme identifies multiple structural variations involved in EGFR activation. *Mutagenesis*, *29*, 341–350.
- Gage, F. H. (2000). Mammalian neural stem cells. *Science*, *287*, 1433–1438.
- Gomez-Randulfe, I., Golan, I., Zumalave, J. A., Pardo-Vazquez, J. L., Arce, V. M., & Costoya, J. A. (2019). Organoids as an improved in vitro model of glioma. *II Annual CIMUS Workshop*, p19.
- Goodwin, C. R., Liang, L., Abu-Bonsrah, N., Hdeib, A., Elder, B. D., Kosztowski, T., Bettgowda, C., Larterra, J., Burger, P., & Sciuabba, D. M. (2016). Extraneural glioblastoma multiforme vertebral metastasis. *World Neurosurg*, *89*, 578–582.
- Haji, G. N. M., da Silva, F. F., de Bellis, B., Lupinacci, F. C. S., Bellato, H. M., Cruz, J. R., Segundo, C. N. C., Faquini, I. V., Torres, L. C., Sanematsu, P. I., Begnami, M. D., Martins, V. R., & Roffé, M. (2020). Aberrant expression of RSK1 characterizes high-grade gliomas with immune infiltration. *Molecular oncology*, *14*, 159–179.
- Hannen, R., Hauswald, M., & Bartsch, J. W. (2017). A rationale for targeting extracellular regulated kinases ERK1 and ERK2 in glioblastoma. *Journal of Neuropathology and Experimental Neurology*, *76*, 838–847.
- Hoffman, H. A., Li, C. H., Everson, R. G., Strunck, J. L., Yong, W. H., & Lu, D. (2017). Primary lung metastasis of glioblastoma multiforme with epidural spinal metastasis: Case report. *Journal of Clinical Neuroscience*, *41*, 97–99.
- Jacob, F., Salinas, R. D., Zhang, D. Y., Nguyen, P. T. T., Schnoll, J. G., Wong, S. Z. H., Thokala, R., Sheikh, S., Saxena, D., Prokop, S., Liu, D. A., Qian, X., Petrov, D., Lucas, T., Chen, H. I., Dorsey, J. F., Christian, K. M., Binder, Z. A., Nasrallah, M., ... Song, H. A. (2020). A patient-derived glioblastoma organoid model and biobank recapitulates inter- and intratumoral heterogeneity. *Cell*, *180*, 188–204.
- Joshi, S. K., Lucic, N., & Zuniga, R. (2015). Molecular pathogenesis of glioblastoma multiforme: Nuances, obstacles, and implications for treatment. *World Journal of Neurology*, *5*, 88–101.
- Jun, H. J., Appleman, V. A., Wu, H., Rose, C. M., Pineda, J. J., Yeo, A. T., Delcuze, B., Lee, C., Gyuris, A., Zhu, H., Woolfenden, S., Bronisz, A., Nakano, I., Chiocca, E. A., Bronson, R. T., Ligon, K. L., Sarkaria, J. N., Gygi, S. P., Michor, F., ... Charest, A. (2018). A PDGFR α -driven mouse model of glioblastoma reveals a stathmin1-mediated mechanism of sensitivity to vinblastine. *Nature Communications*, *2018*(9), 3116.
- Kadoshima, T., Sakaguchi, H., Nakano, T., Soen, M., Ando, S., Eiraku, M., & Sasai, Y. (2013). Self-organization of axial polarity; inside-out layer pattern; and species-specific progenitor dynamics in human ES cell-derived neocortex. *Proceedings of the National Academy of Sciences of the United States of America*, *110*, 20284–20289.
- Larrea, M. D., Hong, F., Wander, S. A., da Silva, T. G., Helfman, D., Lannigan, D., Smith, J. A., & Slingerland, J. M. (2009). RSK1 drives p27Kip1 phosphorylation at T198 to promote RhoA inhibition and increase cell motility. *Proceedings of the National Academy of Sciences of the United States of America*, *106*, 9268–9273.
- Lee, J., Kotliarova, S., Kotliarov, Y., Li, A., Su, Q., Donin, N. M., Pastorino, S., Purow, B. W., Christopher, N., Zhang, W., Park, J. K., & Fine, H. A. (2006). Tumor stem cells derived from glioblastomas cultured in bFGF and EGF more closely mirror the phenotype and genotype of primary tumors than do serum-cultured cell lines. *Cancer Cell*, *9*, 391–403.
- Lee, J. H., Lee, J. E., Kahng, J. Y., Kim, S. H., Park, J. S., Yoon, S. J., Um, J.-Y., Kim, W. K., Lee, J.-K., Park, J., Chang, J. H., Kang, S. G., & Lee, J. H. (2018). Human glioblastoma arises from subventricular zone cells with low-level driver mutations. *Nature*, *560*, 243–247.

- Li, R., Yerganian, G., Duesberg, P., Kraemer, A., Willer, A., Rausch, C., & Hehlmann, R. (1997). Aneuploidy correlated 100% with chemical transformation of Chinese hamster cells. *Proceedings of the National Academy of Sciences of the United States of America*, *94*, 14506–14511.
- Li, X., Wu, C., Chen, N., Gu, H., Yen, A., Cao, L., Wang, E., & Wang, L. (2016). PI3K/Akt/mTOR signaling pathway and targeted therapy for glioblastoma. *Oncotarget*, *7*, 33440–33450.
- Lo, H. W. (2010). Targeting Ras-RAF-ERK and its interactive pathways as a novel therapy for malignant gliomas. *Current Cancer Drug Targets*, *10*, 840–848.
- Lombard, A., Goffart, N., & Rogister, B. (2015). Glioblastoma circulating cells: reality trap or illusion? *Stem Cells International*, *2015*, 182985.
- Louis, D., Perry, A., Reifenberger, G., von Deimling, A., Figarella-Branger, D., Cavenee, W. K., Ohgaki, H., Wiestler, O. D., Kleihues, P., & Ellison, D. W. (2016). The 2016 World Health Organization classification of tumors of the central nervous system: a summary. *Acta Neuropathologica*, *131*, 803–820.
- Mao, H., Lebrun, D. G., Yang, J., Zhu, V. F., & Li, M. (2012). Deregulated signaling pathways in glioblastoma multiforme: Molecular mechanisms and therapeutic targets. *Cancer Investigation*, *30*, 48–56.
- Ostrom, Q. T., Gittleman, H., Truitt, G., Boscia, A., Kruchko, C., & Barnholtz-Sloan, J. S. (2018). CBTRUS statistical report: Primary brain and other central nervous system tumors diagnosed in the United States in 2011–2015. *Neuro-Oncology*, *20*, iv1–iv86.
- Patel, A. P., Tirosh, I., Trombetta, J. J., Shalek, A. K., Gillespie, S. M., Wakimoto, H., Cahill, D. P., Nahed, B. V., Curry, W. T., Martuza, R. L., Louis, D. N., Rozenblatt-Rosen, O., Suvà, M. L., Regev, A., & Bernstein, B. E. (2014). Single-cell RNA-seq highlights intratumoral heterogeneity in primary glioblastoma. *Science*, *344*, 1396–1401.
- Paxinos, G., & Franklin, K. B. J. (2019). *Paxinos and Franklin's the mouse brain in stereotaxic coordinate* (5th ed.). Academic Press.
- Paşca, A. M., Sloan, S. A., Clarke, L. E., Tian, Y., Makinson, C. D., Huber, N., Kim, C. H., Park, J. Y., O'Rourke, N. A., Nguyen, K. D., Smith, S. J., Huguenard, J. R., Geschwind, D. H., Barres, B. A., & Paşca, S. P. (2015). Functional cortical neurons and astrocytes from human pluripotent stem cells in 3D culture. *Nature Methods*, *12*, 671–678.
- Rasnack, D., & Duesberg, P. (1999). How aneuploidy affects metabolic control and causes cancer. *Biochemical Journal*, *340*, 621–630.
- Richards, L., Whitley, O. K. N., MacLeod, G., Cavalli, F. M. G., Coutinho, F. J., Jaramillo, J. E., Svergun, N., Riverin, M., Croucher, D. C., Kushida, M., Yu, K., Guilhamon, P., Rastegar, N., Ahmadi, M., Bhatti, J. K., Bozek, D. A., Li, N., Lee, L., Che, C., ... Pugh, T. J. (2021). Gradient of developmental and injury response transcriptional states defines functional vulnerabilities underpinning glioblastoma heterogeneity. *Nature Cancer*, *2*, 157–173.
- Ried, T., Heselmeyer-Haddad, K., Blegen, H., Schröck, E., & Auer, G. (1999). Genomic changes defining the genesis; progression; and malignancy potential in solid human tumors: A phenotype/genotype correlation. *Genes, Chromosomes & Cancer*, *25*, 195–204.
- Romeo, Y., Zhang, X., & Roux, P. P. (2012). Regulation and function of the RSK family of protein kinases. *Biochemical Journal*, *44*, 553–569.
- Sami, A., & Karsy, M. (2013). Targeting the PI3K/AKT/mTOR signaling pathway in glioblastoma: Novel therapeutic agents and advances in understanding. *Tumour Biology*, *34*, 1991–2002.
- Sanai, N., Tramontin, A. D., Quiñones-Hinojosa, A., Barbaro, N. M., Gupta, N., Kunwar, S., Lawton, M. T., McDermott, M. W., Parsa, A. T., Manuel-García Verdugo, J., Berger, M. S., & Alvarez-Buylla, A. (2004). Unique astrocyte ribbon in adult human brain contains neural stem cells but lacks chain migration. *Nature*, *427*, 740–744.
- Sawada, M., & Sawamoto, K. (2013). Mechanisms of neurogenesis in the normal and injured adult brain. *Keio Journal of Medicine*, *62*(1), 13–28.
- Seoane, J., & De Mattos-Arruda, L. (2014). Escaping out of the brain. *Cancer Discov.* *4*, 1259–1261.
- Seoane, M., Costoya, J. A., & Arce, V. M. (2017). Uncoupling oncogene-induced senescence (OIS) and DNA damage response (DDR) triggered by DNA hyper-replication: lessons from primary mouse embryo astrocytes (MEA). *Scientific Reports*, *7*, 12991.
- Singh, S. K., Hawkins, C., Clarke, I. D., Squire, J. A., Bayani, J., Hide, T., Henkelman, R. M., Cusimano, M. D., & Dirks, P. B. (2004). Identification of human brain tumour initiating cells. *Nature*, *432*, 396–401.
- Smith, L. M., Nesterova, A., Ryan, M. C., Duniho, S., Jonas, M., Anderson, M., Zabinski, R. F., Sutherland, M. K., Gerber, H. P., Van Orden, K. L., Moore, P. A., Ruben, S. M., & Carter, P. J. (2008). CD133/prominin-1 is a potential therapeutic target for antibody-drug conjugates in hepatocellular and gastric cancers. *British Journal of Cancer*, *99*, 100–109.
- Sullivan, J. P., Nahed, B. V., Madden, M. W., Oliveira, S. M., Springer, S., Bhere, D., Chi, A. S., Wakimoto, H., Rothenberg, S. M., Sequist, L. V., Kapur, R., Shah, K., Iafrate, A. J., Curry, W. T., Loeffler, J. S., Batchelor, T. T., Louis, D. N., Toner, M., Maheswaran, S., & Haber, D. A. (2014). Brain tumor cells in circulation are enriched for mesenchymal gene expression. *Cancer Discovery*, *4*, 1299–1309.
- Swift, S., Lorens, J. B., Achacoso, P., & Nolan, G. P. (2001). Rapid production of retroviruses for efficient gene delivery to mammalian cells using 293T cell-based systems. *Current Protocols in Immunology*, *10*, 10.17C.
- Takaishi, S., Okumura, T., Tu, S., Wang, S. S., Shibata, W., Vigneshwaran, R., Gordon, S. A., Shimada, Y., & Wang, T. C. (2009). Identification of gastric cancer stem cells using the cell surface marker CD44. *Stem Cells*, *27*, 1006–1020.
- Taskapilioglu, M. O., Aktas, U., Eser, P., Tolunay, S., & Bekar, A. (2013). Multiple extracranial metastases from secondary glioblastoma: A case report and review of the literature. *Turkish neurosurgery*, *23*, 824–827.
- Todaro, G. J., & Green, H. (1963). Quantitative studies of the growth of mouse embryo cells in culture and their development into established lines. *Journal of Cell Biology*, *17*, 299–313.
- Tomasetti, C., Li, L., & Vogelstein, B. (2017). Stem cell divisions; somatic mutations; cancer etiology; and cancer prevention. *Science*, *355*, 1330–1334.
- Vining, K. H., & Mooney, D. J. (2017). Mechanical forces direct stem cell behaviour in development and regeneration. *Nature Reviews Molecular Cell Biology*, *18*, 728–742.
- Weaver, B. A., & Cleveland, D. W. (2008). The aneuploidy paradox in cell growth and tumorigenesis. *Cancer Cell*, *14*, 431–433.
- van de Wouw, A. J., Janssen-Heijnen, M. L., Coebergh, J. W., & Hillen, H. F. (2002). Epidemiology of unknown primary tumours; incidence and population-based survival of 1285 patients in Southeast Netherlands; 1984–1992. *European Journal of Cancer*, *38*, 409–413.
- Xie, Y., Bergström, T., Jiang, Y., Johansson, P., Marinescu, V. D., Lindberg, N., Segerman, A., Wicher, G., Niklasson, M., Baskaran, S., Sreedharan, S., Everlien, I., Kastemar, M., Hermansson, A., Elfineh, L., Libard, S., Holland, E. C., Hesselager, G., Alafuzoff, I., ...Uhrbom, L. (2015). The human glioblastoma cell culture resource: Validated cell models representing all molecular subtypes. *EBioMedicine*, *2*, 1351–1363.

SUPPORTING INFORMATION

Additional Supporting Information may be found online in the supporting information tab for this article.

How to cite this article: Almengló, C., Caamaño, P., Fraga, M., Devesa, J., Costoya, J. A., & Arce, V. M. (2021). From neural stem cells to glioblastoma: A natural history of GBM recapitulated in vitro. *Journal of Cellular Physiology*, 1–15. <https://doi.org/10.1002/jcp.30409>